# Strain Sensor Design and Fabrication in Instrumented Suspensions

Stanley Kon, Roberto Horowitz
Department of Mechanical Engineering
University of California at Berkeley

December 31, 2004

**Abstract**

Sub-millimeter size strain sensors have been designed, fabricated and tested using micro-electrical-mechanical-system (MEMS) technology. These sensors are fabricated directly on steel wafers, which will be cut and assembled into suspensions later on. The sensors are sufficiently small to fit into the prescribed locations in order to pick up signals only contributing to off-track vibrations at the tip of the suspension. Our results show that the sensors on steel wafers are able to survive the whole fabrication process. The sensors are capable of picking up vibration signals down to 500 nano-strain, which corresponds to 10 nanometer displacement at the tip of the specific suspension we are using. It is estimated that an order of magnitude improvement in resolution can be achieved by reducing the parasitic capacitors and handling the noise carefully.

Keywords: Hard drive disks, Piezoelectric sensor, strain sensor, MEMS

## 1 Introduction

As the hard drive industry continues to increase areal density on hard drives to fulfill the demand in computer and consumer electronic devices, it has been facing much more challenging problems than before. One of the major problems comes from track mis-registration(TMR), which is the distance deviation of the read/write head from the center of a track. TMR may be caused by the vibration resulting from the voice-coil motor(VCM) or air flow excitation. Track runout (tracks are not perfect circles) also contributes to part of TMR. TMR are predicted to be around 5 nanometers ($3\sigma$) for 1 Gbit per square inch density.

Li[1][2] has shown that smaller TMR can be achieved by using dual-stage actuation and implementing vibration suppression control algorithms. In addition to the traditional voice-coil-motor (VCM) only actuation in hard drives, two PZT strips are attached to a hard drive suspension. One of them was used as a sensor and the other one as the second stage actuator. The vibration signal picked up by the PZT sensor was fed back to control both low-frequency motions using the VCM and high frequency compensations using the PZT actuator. Although improved performance was obtained by this configuration, it has several drawbacks. First, the PZT strips are much thicker than suspensions itself. Suspension dynamics can be significantly changed as a result. Second, while PZT strips are too big for suspensions dynamics,

they are too small to be easily attached to suspensions . It is difficult to precisely place the sensors on the desired locations if installed manually. It has been shown [3] that there are only few sweet spots, typically within few hundred microns in size, on the suspension that provide vibration signals closely proportional to off-track motions at the tip of the suspension. Meanwhile, the non-off-track signal of vibration modes that do not contribute to TMR must be kept as small as possible so that they do not increase the servo load. Although manually-attached PZT sensors do pick up suspension vibration signals, the signals contain both off-track and non-offtrack informations because they cover too large an area.

Piezoelectric sensors, which are much smaller and thinner than PZT sensors, have been prototyped on steel to produce instrumented suspension. These sensors can be built at optimal locations on the real suspension and will give us the ideal signals that contain only information of off-track vibration. Since the signals picked by these dedicated sensors are not contaminated by run-out as position-error-signals (PES), they can be used by various control algorithms to increase not only the positioning accuracy but also system robustness of a new dual stage servo system [4]. In our new configuration, a new gap-closing electrostatic actuator is designed and fabricated using MEMS technology. The MEMS actuator will replace the PZT as the second stage actuator. In this report, we focus on sensor fabrication, discuss the difficulties we encountered in the non-standard MEMS process and the experimental results.

## 2 Piezoelectric Theory

Any piezoelectric material behavior can be described by two equations, one for direct piezoelectric response and the other one for indirect piezoelectric response. Equation (1) describes how mechanical energy can be injected into a electrical system via an additive term, $d_{ij}T_j$. Similarly, equation (2) describes the indirect piezoelectric response by adding an additional term, $d_{ji}E_j$, to the mechanical stress-strain equation.

$$D_i = d_{ij}\ T_j + \varepsilon_{ii}\ E_i \tag{1}$$

$$S_j = s^E_{kj}\ T_j + d_{ji}\ E_i \tag{2}$$

In these equations, $D_i$, $S_j$, $T_j$, $E_i$, $d_{ij}$, $\varepsilon$, and $s^E_{kj}$ denote electric displacement, mechanical strain, mechanical stress, electric field, piezoelectric constants, material permittivity and elastic compliance, respectively. Matrices $d_{ij}$ and $s^E_{kj}$ are full matrices in general and are material dependent. However, for ZnO under the assumption that the film has isotropic in-plane properties, equations (1) and (2) can be reduced to the following equations:

$$\begin{pmatrix} D_1 \\ D_2 \\ D_3 \end{pmatrix} = \begin{pmatrix} 0 & 0 & 0 & 0 & d_{15} & 0 \\ 0 & 0 & 0 & d_{15} & 0 & 0 \\ d_{31} & d_{31} & d_{33} & 0 & 0 & 0 \end{pmatrix} \begin{pmatrix} \tau_{11} \\ \tau_{22} \\ \tau_{33} \\ \tau_{23} \\ \tau_{13} \\ \tau_{12} \end{pmatrix} + \varepsilon_0 \begin{pmatrix} \varepsilon_{11} & 0 & 0 \\ 0 & \varepsilon_{11} & 0 \\ 0 & 0 & \varepsilon_{33} \end{pmatrix} \begin{pmatrix} E_1 \\ E_2 \\ E_3 \end{pmatrix} \tag{3}$$

$$\begin{pmatrix} S_{11} \\ S_{22} \\ S_{33} \\ S_{23} \\ S_{13} \\ S_{23} \end{pmatrix} = \begin{pmatrix} s_{11} & s_{12} & s_{13} & 0 & 0 & 0 \\ s_{12} & s_{11} & s_{13} & 0 & 0 & 0 \\ s_{13} & s_{13} & s_{33} & 0 & 0 & 0 \\ 0 & 0 & 0 & s_{55} & 0 & 0 \\ 0 & 0 & 0 & 0 & s_{55} & 0 \\ 0 & 0 & 0 & 0 & 0 & s_{66} \end{pmatrix} \begin{pmatrix} \tau_{11} \\ \tau_{22} \\ \tau_{33} \\ \tau_{23} \\ \tau_{13} \\ \tau_{12} \end{pmatrix} + \begin{pmatrix} 0 & 0 & d_{31} \\ 0 & 0 & d_{31} \\ 0 & 0 & d_{33} \\ 0 & d_{15} & 0 \\ d_{15} & 0 & 0 \\ 0 & 0 & 0 \end{pmatrix} \begin{pmatrix} E_1 \\ E_2 \\ E_3 \end{pmatrix} \tag{4}$$

where the $x_3$ axis lies in parallel with the ZnO c-axis. In our case, the c-axis is the direction of the electric field during deposition, which is perpendicular to the film. To use a ZnO film as strain sensors, we further assume that $\tau_{33}$ is negligible. Because we only deposit electrodes on the top and bottom of the ZnO film, we also assume the electrodes will only pick up charges as a result of $d_{31}$. There is no external electric field as we do not apply any external voltage. Under this condition, equation (3) can be reduced to

$$D_3 = d_{31}(\tau_{11} + \tau_{22}) \tag{5}$$

Equation (4) is nothing but a standard stress-strain relation without the presence of external electrical field. Assuming $S_{33}$ is negligible, using the stress-strain relation and noticing that

$$D_3 = \frac{Q_3}{A} = \frac{\varepsilon_{33} V}{t} \tag{6}$$

where V is the voltage generated, Q is the charge generated, and t is film thickness, equation (5) can be expressed as

$$V = \frac{d_{31} t}{\varepsilon_{33}}(C_{11}S_{11} + C_{22}S_{22}) = \frac{d_{31} t}{\varepsilon_{33}} C_{11}(S_{11} + S_{22}) \tag{7}$$

where $C_{ij}$ are the constants in the standard stress-strain relation, $\tau_{ij} = C_{ijkl}\ S_{kl}$. Theory predicts that in order to produce the best sensitivity in terms of voltage, one needs to choose a material with high piezoelectric constant and low permittivity. A thicker film also helps to increase sensitivity. The table below lists comparisons between the most common piezoelectric material Lead Zirconate Titanate (PZT) and ZnO, which is the material used for the sensor fabrication in this project. Although PZT has more than one order of magnitude higher a piezoelectric constant than ZnO, it has a much smaller permittivity. As a result, ZnO produces a higher voltage output than PZT when it is used as a sensor.

| | $d_{31}$ (pC/N) | $C_{11}$ (GPa) | $\varepsilon_{33}$ |
|---|---|---|---|
| PZT | 123 | 53 | 1700 |
| ZnO | 5.2 | 209 | 11 |

Table 1: Material comparison between PZT [1] and bulk ZnO [5].

# 3 Fabrication

## 3.1 Sensors Fabricated on Silicon Wafers

A cross-sectioned view of the sensor is shown to the left of Fig 2. We start with a <100> silicon wafer. After wafer cleaning, we apply a 0.6 um spin-on-glass(SOG). This step is not critical for sensors on silicon substrates but is very important for producing working sensors on steel wafers. Not only does it passivate the steel wafers but it also planarizes the steel wafer surface for growing ZnO with good crystal structure. As shown in Fig 1, steel wafers are extremely rough in micro fabrication terms. SOG does a good job in planarizing local roughness, although some waviness can still be measured.

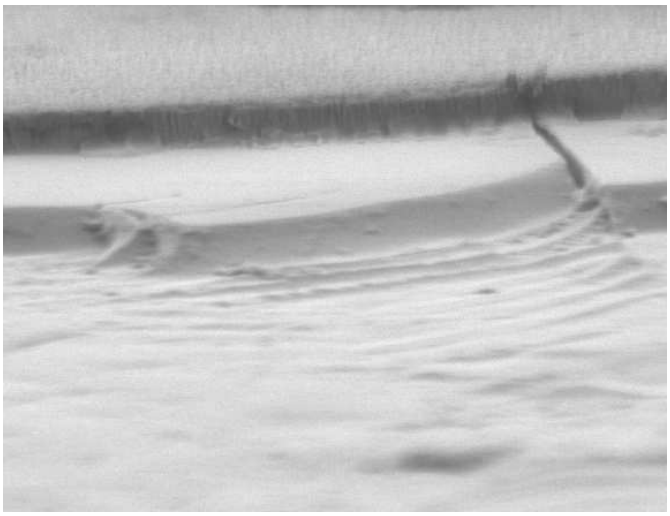

Figure 1: A ZnO film on a SOG film on a steel substrate

After SOG deposition, the bottom electrode is deposited and patterned. Aluminum is chosen for the bottom electrode because it is more conductive than chrome and cheaper than gold. After the bottom electrode is formed, a 0.8 um thick ZnO film is deposited on the substrate using the sputtering machine MRC8600. The machine is pumped down to sub $10^{-6}$ torr pressure before Ar and $O_2$ are introduced. The pressure for each gas ranges from 0.0034 torr to 0.0050 torr, producing ZnO films with very similar piezoelectric responses. The substrate is heated to 350 degree Celcius and 200 W forward power is applied for sputtering. The deposition rate on averaged is 150 nm/min. Deposition rate is typically higher at the center of the wafers and gradually decreases towards the edge. A second aluminum layer is evaporated directly on top of the ZnO film. This aluminum layer is patterned by $K_3Fe(CN)_6$:KOH:$H_2O$ = 10:1:100 mixture to form the top electrode, followed by ZnO etching using the $CH_3COOH$:$H_3PO_4$:$H_2O$ = 1:1:30 solution. Next, another layer of SOG is spun on for passivation. Finally, the SOG contact holes are opened by plasma dry etch and then the final aluminum deposition and patterning completes the process.

As can be seen from equation (7), the output voltage is proportional to the film thickness. It would be ideal to deposit the film as thick as possible, but this is not practical in real fabrication because it

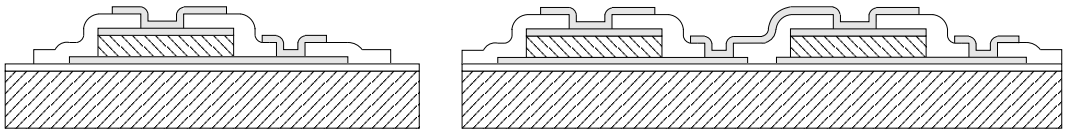

Figure 2: Process flow

would require a much longer time to deposit and film properties become worse with increasing thickness [6]. In other words, the first few micron of film has good piezoelectric properties as it grows very good column structures. Unfortunately, these columns tends to grow sideways as the film gets thicker. Thus, we do not get a response proportional to thickness in reality. To work around this problem, we propose to connect adjacent sensors together to make them work effectively as a thick sensor, as shown on the right of Figure 2. This layout, however, is done at the cost of total sensor area; it may be larger than the area identified by the sensor optimization results.

### 3.2 Sensors Fabricated on Steel wafers

Steel wafers are very different than standard silicon wafers. They are easily oxidized at high temperatures, and its mechanical properties may change after going through different temperature process. Steel wafers are also much thinner and rougher than standard silicon wafers; we use both 80-um and 30-um thick steel wafers. At either thickness, the wafers are so thin that they are easily deformed. For example, the vacuum on the chuck that is used to hold wafers in place for spin-coating deforms steel wafers and leave groves on the wafer surface after spinning. Steel wafers should be bonded to silicon wafers during certain processing steps. We tried to bond steel wafers to silicon wafers using photoresist(PR), the most common material for between-process bonding. However, PR proved unsuitable for our purpose because some deposition processes, such as ZnO sputtering, require as high as 350 degree Celcius and will burn PR. Not only does the burned PR contaminate the chamber but it is also extremely hard to remove. Thus, bonding should be temporary and the wafers need to be released before under going into certain processes. As wafer-scale PR bonding takes a full day to be released, we have introduced water bonding to temporarily bond steel wafers to silicon wafers. The amount of water between handle wafer and steel wafer determines how well they stick to each other. By carefully control the amount of water left between wafers, the steel wafer can be attached to handle wafer so well that there is no problem at all even during spin coating at more than 5000 revolution per minute (RPM), yet it is also very easy to separate two wafers by heating them up to 100 degree. This greatly simplifies steel wafer handling, especially during lithography steps.

Another attribute that makes steel wafers difficult to process is their thermal expansion coefficient. The thermal expansion coefficient is much larger than all other standard micro fabrication materials. This is especially detrimental after ZnO deposition because of the relatively high temperature during the

process. As steel wafers are much thinner than silicon wafers and carry the larger expansion coefficient, it is not unexpected to find that the steel wafers buckle after deposition. We observe that 80-um wafers have the worst residual stress problems because these substrates are thickest relative to the ZnO film. The deposited film starts to crack and peel off wafers even before the wafers are removed from the chamber. Using thinner steel wafers alleviates stress problem but film cohension is still marginal; cracks can still be initiated if the wafer is heated for too long a time in the chamber.

The fabrication process on steel wafers has been modified slightly from that on silicon wafers to solve this problem. An additional mask is introduced to pattern ZnO before aluminum is deposited. Although aluminum films are generally considered as low stress films, they induce a compressive residual stress on the ZnO film. Since the residual stress is already marginal on the ZnO film, the additional stress causes the ZnO film to peel of the substrate. Patterning the ZnO film first solves this problem by confining residual stress within the patterned area and preventing any crack from propagating across the wafer. The additional mask also solves the undercut problem observed in the process for silicon wafers. Since the ZnO etchant attacks the ZnO film laterally much faster than it does vertically, it undercuts the ZnO film underneath the top electrode when a single mask is used to pattern both top electrode and the ZnO film. As a result, a portion of the top electrode is unsupported and may short out to the bottom electrode during later processing, causing sensors to respond very differently across the wafer. The additional mask enables us to compensate for this and make sensors response more consistent.

# 4 Experiment

## 4.1 Circuit

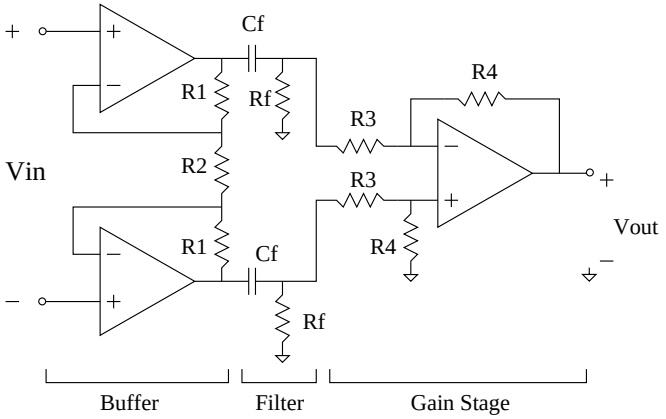


Figure 3: Sensing Circuit

As sensor size is reduced, the sensor generates fewer less charge, although the voltage stays the same, as can be deduced from eq (7). The amount of charge or current generated by sub-millimeter sensors is so tiny that it does not supply enough bias current for ordinary operational amplifiers. A buffer circuit is needed in order to deal with this small amount of current. The circuit is composed of a signal conditioning

buffer followed by an amplifier. The buffer is a differential input voltage to voltage converter. It takes the tiny voltage difference across the sensor and converts it to a differential voltage source. This buffer also amplifies the signal by a factor of ten. The second stage of this circuit uses several high pass filters to filter out low frequency, particularly 60 Hz noise, and then amplifies the signal one hundred times. This circuit can resolve around 20 micro voltage input voltage if only thermal and amplifier noise are present though it has 50 to 100 micro volt resolution in practice because of environmental noise.

### 4.2 Experiment Setup

Our $d_{33}$ test shows ZnO films have similar piezoelectric response on both silicon wafers and steel wafers, so $d_{31}$ tests are mostly performed on silicon wafers due to their greater availability. Furthermore, steel wafers are too flexible to handle easily and it is difficult to cut steel wafers into small pieces without plastically deforming some part of those pieces when preparing for experiments. Therefore, the sensor responses on steel wafers are predicted according to those on silicon wafers under the assumption of the same $d_{33}$ responses. To test sensitivity, a wafer is cut into cantilevers and they are clamped on a fixed base. As shown in Fig 4, wires are glued to the strips using conductive epoxy in order to pass the vibration signal to the circuit. The first free vibration mode of the strip, once excited, can be easily measured on the oscilloscope, while a laser Doppler vibrometer (LDV) is focused on the tip of the strip to measure end displacement. The first free vibration mode can be calculated by the following equation:

$$y(x) = C_n[\sin\beta_n x - \sinh\beta_n x - \alpha_n(\cos\beta_n x - \cosh\beta_n x)] \tag{8}$$

$$\text{where} \quad \alpha_n = \frac{\sin\beta_n L + \sinh\beta_n L}{\cos\beta_n L + \cosh\beta_n L} \tag{9}$$

Strain is evaluated by differentiating the above equation twice,

$$\varepsilon = \frac{\bar{y}}{\rho} = \bar{y}\,\frac{d^2y}{dx^2} \tag{10}$$

where $\varepsilon$, $\bar{y}$, $\rho$, $x$ and $y$ denote the strain, the distance to neutral axis, radius of curvature, the distance to base and the displacement, respectively. From the LDV signal and the amplified sensors signal, the piezoelectric constant $d_{31}$ can be evaluated using the following equation:

$$V = \frac{d_{31}tE}{\varepsilon_r}S \;\Rightarrow\; d_{31} = \frac{\varepsilon_r V}{tES} \tag{11}$$

### 4.3 Results

A wafer scale unpatterned characterization of ZnO film is performed before measuring the sensor response. It is found that, using exactly the same experimental setup, a smaller response is measured as the sensors become smaller due to the parasitic capacitance. Wafer scale characterization minimizes this problem and the measured piezoelectric response is closer to the true value, because ZnO covering an entire wafer produces much more charge and has a much larger capacitance than the patterned sensrs. In this test,

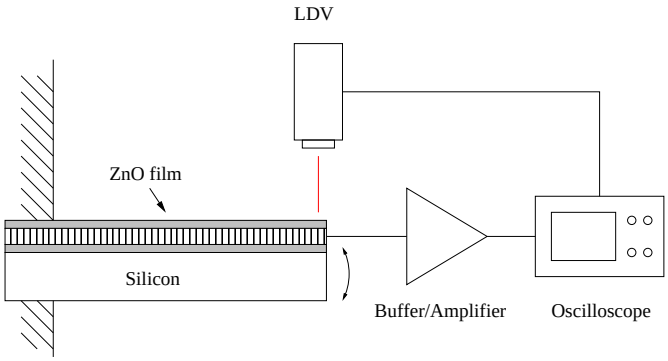


Figure 4: Experimental setup for ZnO piezoelectric response measurement.

the beam is completely covered with ZnO film. Since there is a strain distribution along the length of the beam, we averaged the strain to calculate the upper bound of $d_{31}$ and used the strain at the base for lower bound of $d_{31}$, giving estimates of 1.37 and 0.72 $pC/N$, respectively. This response agrees with most of the literatures.

After wafer scale characterization, a similar test is performed on a cantilever beam cut from the wafer, with a 380 $\mu m$ by 380 $\mu m$ sensor at the base. Figure 5 shows the sensors ,which are half of the size as the one we used for testing, on a silicon wafer and a steel wafer. The sensor is able to resolve 0.5 mV output with a corresponding strain of 500 nano strain. The calculated piezoelectric constant $d_{31}$ is 0.25 $pC/N$, a factor of four smaller than the value from wafer scale characterization. The reduction in the measured piezoelectric response is attributed to parasitic capacitor. In the current experimental setup, the sensor signal is passed to the circuit using coaxial cable. It is estimated that the coaxial cable has around 50 $pF$, while the measured and theoretical capacitance of the sensor are only 15 and 12 $pF$, respectively. Since the parasitic capacitor is in parallel with the sensors, it is reasonable that the measured response is diminished by a factor of four or five. It is expected that fifty nano strain resolution can be achieved by shorten wire length between the sensor and the circuit to reduce the parasitic capacitors from the cable and by carefully handling the noise.

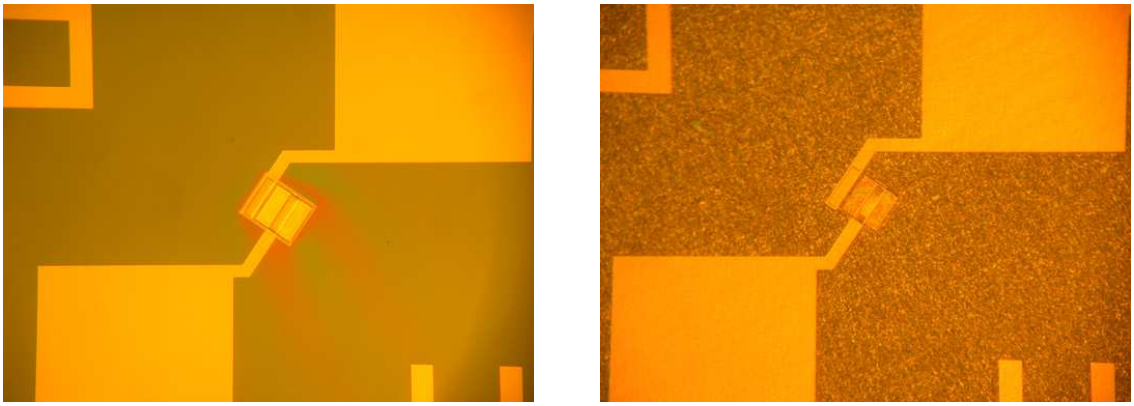

(a) A sensor on a silicon substrate.

(b) A sensor on a steel substrate.

Figure 5: 200 $\mu m$ by 200 $\mu m$ sensors on silicon and steel substrate

## 5 Conclusion

ZnO piezoelectric strain sensors have been fabricated on silicon and steel substrates for vibration sensing. Despite steel wafers' rougher surface and large thermal expansion coefficient, ZnO sensors on steel wafers show similar piezoelectric response to those on silicon wafers. Sensor resolution to 500 nano strain is achieved for 380 *um* square sensors. Further improvement in experimental setup and noise control are needed for even better resolution or smaller sensors.

## References


[1] Yunfeng Li, Horowitz R, and Evans R. Vibration control of a pzt actuated suspension dual-stage servo system using a pzt. *IEEE Transactions on Magnetics*, 39(2):932–7, March 2003.

[2] Yunfeng Li, Marcassa F, Horowitz R, Oboe R, and Evans R. Track-following control with active vibration damping of a pzt-actuated suspension dual-stage servo system. volume 3, pages 2553–9. IEEE, 2003.

[3] Kenn Oldham, Stanley Kon, and Roberto Horowitz. Fabrication and optimal strain sensor placement in an instrumented disk drive suspension for vibration suppression. *CML report*, 2004.

[4] Xinghui Huang, Ryozo Nagamune, Roberto Horowitz, and Yunfeng Li. Design and analysis of a dual-stage disk drive servo system using an instrumented suspension. In *Proc of American Control Conference*, volume 4, pages 535–540, 2004.

[5] Hari Singh Nalwa, editor. *Handbook of Thin Film Materials*, volume 3. Academic Press, 2002.

[6] Yong Eui Lee, Young Jin Kim, and Hyeong Joon Kim. Thickness dependence of microstructural evolution of zno films deposited by rf magnetron sputtering. *Journal of Materials Research*, 13(5):1260–5, May 1998.